Advanced Engineering Materials

Hybrid Filtration Membranes incorporating Nanoporous Silica within a Nanoscale Alumina Fibre Scaffold

--Manuscript Draft--

Manuscript Number:	adem.201500220R1
Full Title:	Hybrid Filtration Membranes incorporating Nanoporous Silica within a Nanoscale Alumina Fibre Scaffold
Article Type:	Full Paper
Section/Category:	
Keywords:	Scaffold; Hybrid; membrane; nanofibres; ultrafiltration
Corresponding Author:	Trevor William Clyne, PhD The Gordon Laboratory Cambridge , UNITED KINGDOM
Additional Information:	
Question	**Response**
Please submit a plain text version of your cover letter here. **If you are submitting a revision of your manuscript, please do not overwrite your original cover letter. There is an opportunity for you to provide your responses to the reviewers later; please do not add them here.**	This paper is being submitted to Adv. Eng Materials. It is a development of preliminary work published 3 years ago in Adv. Eng Materials. It concerns the creation of membranes for ultra-filtration, using alumina nano-fibres and sol gel processing.
Corresponding Author Secondary Information:	
Corresponding Author's Institution:	The Gordon Laboratory
Corresponding Author's Secondary Institution:	
First Author:	Veronica Su, PhD
First Author Secondary Information:	
Order of Authors:	Veronica Su, PhD
	Trevor William Clyne, PhD
Order of Authors Secondary Information:	
Abstract:	Membranes were produced from as-received nanoscale alumina fibres, having diameters of the order of 10 nm. These fibres were dispersed in a liquid, followed by sedimentation, to produce two types of membrane - one comprising a duplex structure of well-dispersed fibres and fibre micro-bundles and the other composed entirely of micro-bundles. These membranes were also used as scaffolds for incorporation of silica, using a sol-gel method, to produce 'hybrid' forms. The fibre and pore architecture within the membranes, as well as their filtration and separation properties, have been investigated. Correlations have been established between this architecture and membrane transport properties. The filtration and separation efficiencies of the membranes have been assessed with two ionic dyes of similar molecular weight, but opposite charge. The successful separation of these two dyes is attributed to surface electrical effects within nanopores. These hybrid membranes were found to give an excellent combination of fine scale filtration efficiency and high permeability.

Submitted to Adv. Eng. Materials, April 2015

Hybrid Filtration Membranes incorporating Nanoporous Silica within a Nanoscale Alumina Fibre Scaffold

VMT Su & TW Clyne[†]

Department of Materials Science & Metallurgy
Cambridge University
27 Charles Babbage Road, Cambridge CB4 2ED, UK

Abstract

Membranes were produced from as-received nanoscale alumina fibres, having diameters of the order of 10 nm. These fibres were dispersed in a liquid, followed by sedimentation, to produce two types of membrane – one comprising a duplex structure of well-dispersed fibres and fibre micro-bundles and the other composed entirely of micro-bundles. These membranes were also used as scaffolds for incorporation of silica, using a sol-gel method, to produce 'hybrid' forms. The fibre and pore architecture within the membranes, as well as their filtration and separation properties, have been investigated. Correlations have been established between this architecture and membrane transport properties. The filtration and separation efficiencies of the membranes have been assessed with two ionic dyes of similar molecular weight, but opposite charge. The successful separation of these two dyes is attributed to surface electrical effects within nanopores. These hybrid membranes were found to give an excellent combination of fine scale filtration efficiency and high permeability.

Keywords: Scaffold; hybrid; membrane; nanofibres; ultrafiltration.

Introduction

Inorganic membranes have received extensive attention for gas and liquid separation, since they can be used in harsh conditions (unlike polymeric membranes). There are often two main components in inorganic membranes. One is the ***active component***, where the actual filtration takes place, and the other is the ***support component***, providing the mechanical strength needed to withstand handling and service conditions. The active component requires precise control of pore size, shape and surface chemistry [1, 2]. Silica and silicates are commonly employed, partly because such species can readily be introduced using the sol-gel approach [3]. However, the high

[†] Corresponding author:
tel: 0044 1223 334332
e-mail: twc10@cam.ac.uk

surface to volume ratio of such active components tends to result in a lack of mechanical integrity and hence the need for a support layer or network.

The support component must be mechanically robust, as well as sufficiently permeable to allow flow through the active component. The most common configuration of such membrane systems is a 3-layer asymmetrical structure, with an α-Al_2O_3–based substrate, a γ-Al_2O_3-based intermediate layer, supporting an uppermost active layer such as silica [4, 5]. However, there are problems with many current configurations. Support assemblies of porous α-Al_2O_3 are often relatively dense and have low permeability [4]. Also, the intermediate layers tend to delaminate during prolong usage [5]. The active layer is usually very thin and often prone to cracking.

Using fibrous material in filtration applications often allows attractive combinations of high porosity (giving both high permeability and low stiffness) and relatively high strength. A low stiffness tends to confer good strain tolerance and hence good handling properties. This is also favoured by fibre segments (between "joints" in the network) having high aspect ratios [6]. For fibre networks, all surfaces tend to be in contact with (flowing) fluid, with no "dead end" pores. Furthermore, there is a general correlation between the scale of the fibre diameter and the scale of species filtered [7]. Fine fibres thus lead to improved efficiency of interaction between internal surfaces and permeating fluids, which is important for both catalysis and separation processing. A relatively high fibre aspect ratio promotes mechanical inter-locking, leading to sheets that are mechanically robust, although it is certainly not necessary for the fibres to be continuous or to have a very high aspect ratio. Obviously, a very fine fibre can be quite short, while maintaining a relatively high aspect ratio, which may be advantageous during membrane production. Overall, there are major incentives to use (fine) fibres in membranes.

In a previous publication [8], production of a novel nanoscale alumina fibre membrane was reported, using a variant of the established (wet lay-up) technique employed in the paper industry. These fibres have a diameter of ~5-10 nm and are single crystals of γ-Al_2O_3. They are produced in large "mats", at relatively low cost, with individual fibres being highly aligned and having lengths of up to about 150 mm (ie aspect ratios of more than 10^4). The membranes were made by dispersion of the as-received fibres in an aqueous medium, sedimentation and filtration. They were then dried and heat treated, to generate some bonding between contacting fibres. This resulted in fine fibrous networks [8], having average pores sizes of around 10-15 nm and porosity levels of about 85-90%. In the present paper, work is described on incorporating nano-porous silica into the interstices within such networks, to form hybrid membranes, and on characterising their structure and properties.

2 Experimental Procedures

2.1 Materials

The fibres were supplied by Nafen™. Tetraethyl Ortho Silicate (TEOS) and Pluronic (P123) were obtained from Sigma Aldrich. Hydrochloric acid (HCl, 1M standard solution) was obtained from Acrcos Organics and general purpose grade ethanol from Fisher Scientific. De-ionised (DI) water was from Brenntag.

2.2 Production of Fibre Assemblies

2.2.1 Homogeneous Fibre Bundles

The as-received fibre mats were cut into 10 × 10 × 30 mm blocks, using a razor blade. They were placed in a Petri dish and wetted thoroughly with DI water. A vacuum pump was used to draw out trapped air within the bundles and promote water penetration. Excess water was removed with a pipette and the samples were dried at 80˚C overnight. The volume fraction of fibre in the assembly increased significantly during the drying process, as the fibres moved closer together. This was easily inferred from the observed shrinkage of the bundles in the transverse direction. This "homogeneous bundle" material was treated as a control, to assist in study of the 'duplex' nature of membranes containing both dispersed fibres and fibre bundles (see §2.2.2).

2.2.2 Duplex and Micro-bundle Membranes

Procedures for manufacturing membranes were developed from previously-employed procedures [8]. Membranes were produced by first creating a suspension of fibres (extracted from as-received fibre mats) in DI water. This suspension was agitated with a magnetic stirrer for different periods and then decanted into a vessel with either a Polyethylene Sulphone mesh (pore size ~ 0.2 μm) or a 100 μm stainless steel mesh at the bottom, through which the liquid flowed. The PES mesh retained most of the fibres, producing a "duplex" structure (comprising a lower layer of well-dispersed fibres and an upper layer of fibre micro-bundles). The 100 μm stainless steel mesh only retained about 75% of the fibres, mostly in the form of micro-bundles.

The meshes were removed and the membranes compressed and dried between two aluminium plates at 130˚C for 10 h. After drying, the membranes were heat treated at 700˚C, with a heating rate of 2˚C min^{-1} and a dwell time of 2 h. These membranes were in the form of circular disks, with diameters up to 100 mm. Their thickness was typically about 350 μm. They were found to be mechanically robust and could be cut with scissors.

2.2.3 Silica-containing Membranes

According to Zhao et al [9], the diameter of pores in silicate and silica structures are related to the type of surfactant used to make the sol-gel mixture. The formulation (including experimental

conditions) adopted for the current study [9, 10] was based on the Pluronic surfactant, P123. This surfactant is known [9] to produce silicate-derived structures with pore diameter of ~9 nm.

Both duplex and micro-bundle membranes were employed as scaffolds for incorporating silica via a sol-gel technique. The sol-gel mixture was created in the molar ratios [10] of 1 TEO: 0.0096 P123: 6 DI H_2O: 8.8 ethanol: 0.001 HCl. The TEO, HCl, DI water and half of the ethanol were stirred at 50˚C for 1 hour, using a magnetic stirrer. After 50 min, heating was stopped and the solution was allowed to cool to room temperature, whilst stirring continued for another 10 min. The solution of P123, dissolved in the other half of the ethanol, was added drop-wise and stirring was continued for a further 3 hours at room temperature. The sol-gel mixture was spread over one side of the membrane, using a disposable pipette. The coating was applied so that a smooth layer was seen on the surface of the membrane, without spilling over the edge.

The coating permeated the surface of the membrane and was left to undergo evaporation-induced self-assembly (EISA) [11] for 24 hours at room temperature. EISA is a spontaneous organization of materials through non-covalent interactions (hydrogen bonding and van der Waals forces), with no external intervention. For silica formation, suppression of inorganic siloxane polymerisation during coating is essential. This was achieved under acidic conditions at a hydronium ion concentration corresponding closely to the iso-electric point of colloidal silica [11]. By turning off siloxane condensation, cooperative silica-surfactant self-assembly can proceed. Subsequent heating was carried out at 1˚C min^{-1}, up to 500˚C, with a dwell time of 3 h to remove the surfactant P123 and solidify the silica skeleton, resulting in a meso-porous silica structure within the homogeneous or duplex fibre networks. The amount of silica in both types of membrane was calculated by weighing them before and after the sol-gel treatment.

2.3 Membrane Characterisation

Fibre assemblies were examined using a scanning electron microscope (JEOL JSM 6340F), with a field emission gun operating at 5 kV. These samples were coated with Au-20%Pd before examination. This coating caused the apparent fibre diameter in SEM images to be significantly increased. This is difficult to avoid, since, in the absence of a conductive coating, the fibres have a strong tendency to become charged in the SEM. In order to study individual fibres in detail, transmission electron microscope (TEM) studies were carried out using a JEOL JEM2100, with an accelerating voltage of 200 kV. The TEM images were used to assess the true diameter of the fibres, while SEM images were useful for examination of the architecture of the fibre network in the membranes. Elemental compositions of silica-containing membranes were obtained using Energy Dispersive X-ray Spectroscopy (EDX) in the SEM, over a sample area of 2000 μm^2.

The volume fraction of fibres, *f*, in each membrane was obtained via a simple weighing operation, taking the density of the fibres to be 3.89 g cm^{-3} and that of the silica to be 2.65 g cm^{-3}. A Sartorius CP224S balance was used for this purpose, with a precision of ±10 µg. Membrane thicknesses were measured with digital callipers, while the in-plane dimensions were obtained using a ruler. It may be noted that, while there was some variation in the value of *f* between different membranes, it was generally of the order of 10-15%, which is fairly typical of an approximately isotropic (or planar random) fibre network material.

Specific surface areas and pore sizes of the membranes were determined using the Brunauer-Emmett-Teller (BET) [12] and Barret-Joyner-Halenda (BJH)[13] methods respectively, based on the gas adsorption isotherm. A MicroMeritics TriStar 3000 (Norcross, GA, USA) was used, with detection range [14] between pore sizes of ~1.7 – 300 nm. The samples were thoroughly dried in nitrogen atmosphere at 110˚C overnight. Mercury intrusion porosimetry was conducted using a MicroMeritics AutoPore IV (Norcross, GA, USA). This was used to evaluate overall porosity, with a detection range of pore sizes down to ~7 nm.

2.4 Permeation Characterisation

Experimental permeation studies were conducted with the set-up shown schematically in Fig.1. The membranes were supported in a polycarbonate filter holder, using previously-developed procedures [8]. A cross-flow condition was generated with a peristaltic pump. The pressure drop across the membrane was approximately 0.1-0.7 bar. Corresponding volumetric flow rates were measured.

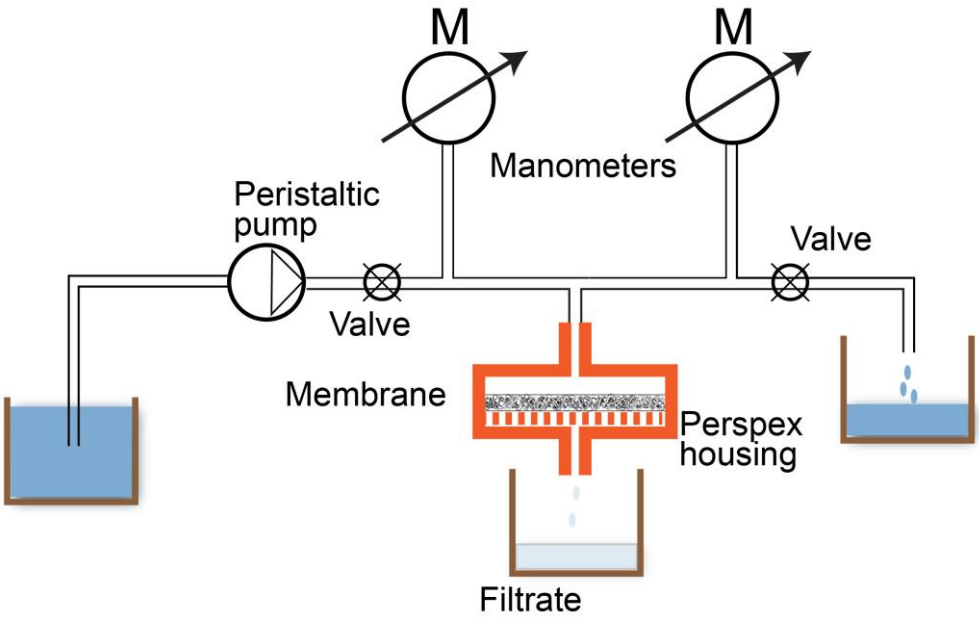

Fig.1 Schematic depiction of the set-up employed for measurement of the membrane permeability and the filtration efficiency.

These two parameters are related via Darcy's Law, giving the volumetric flow rate, Q (in $m^3\ s^{-1}$), and the corresponding flux, q (in $m^3\ m^{-2}\ s^{-1}$), in terms of the pressure gradient ($\Delta P/h$), the dynamic viscosity, η (in Pa s) and the specific permeability, κ (in m^2)

$$q = \frac{Q}{A} = \frac{-\kappa}{\eta}\left(\frac{\Delta P}{h}\right) \tag{1}$$

where h is the membrane thickness and A is the nominal sectional area through which the flow takes place. The specific permeability can therefore be expressed as

$$\kappa = \frac{-q\eta h}{\Delta P} \tag{2}$$

The viscosity of the fluid (water) was taken as 8.9×10^{-4} Pa s. This allowed the permeability to be obtained from the measured membrane thickness and volumetric flow rate. Values of the specific permeability obtained experimentally via Eqn.(2) were compared with those predicted using the Carman-Kozeny equation [15, 16], which is an empirical expression based on the porosity, ϕ, and the specific surface area, S (in $m^2\ m^{-3}$) of the porous medium

$$\kappa = \frac{\phi^3}{\lambda\left(1-\phi^2\right)S^2} \tag{3}$$

where λ is a dimensionless constant, which typically has a value of about 5. For an assembly of long fibres, of diameter D, the value of S is given by

$$S = \frac{N\pi DL}{L} = N\pi D = \left(\frac{4f}{\pi D^2}\right)\pi D = \frac{4f}{D} \tag{4}$$

which is based on a bundle of fibres of length L, with N fibres per unit area. The specific permeability can therefore be expressed as

$$\kappa = \frac{\left(1-f\right)^3}{5f^2}\left(\frac{D}{4f}\right)^2 = \frac{\left(1-f\right)^3 D^2}{80f^4} \tag{5}$$

This expression is used in the present work to predict the specific permeability as a function of the fibre diameter and volume fraction.

2.5 Filtration and Separation Efficiency

The filtration efficiency of the membranes was assessed using the same set-up (Fig.1), with a dyed liquid. Two synthetic dyes were used – namely Trypan Blue (MW ~ 873, average molecular diameter ~ 5 nm) and Methylene Blue (MW ~ 320, average molecular diameter ~ 2 nm). The intensity of the colour of the filtrate was used as a semi-quantitative guide to the filtration efficiency of the membrane concerned. The separation efficiency of the membranes was assessed

by visually detecting the separation of a solution containing two synthetic ionic dyes, Methylene Blue and Methyl Orange. Positive separation was inferred when the mixture of dyes, which was initially green, separated into an orange filtrate, with the retention of a blue dye on the membrane.

3 Fibre and Pore Architecture within the Membranes

3.1 Microstructure of Homogeneous Fibre Bundles

The material formed as described in §2.2.1 contained a high volume fraction of aligned fibres. The inter-fibre spacing within such bundles is obviously relevant to flow through them. Assuming an hexagonal distribution of fibre centres in the transverse plane, the minimum inter-fibre spacing, *s*, is given by:

$$s = D\left[\left(\frac{\pi}{2f\sqrt{3}}\right)^{1/2} - 1\right] \qquad (6)$$

where D is the fibre diameter and f is the fibre volume fraction. The fibre volume fractions (estimated from measured densities) were 5.5% and 26% respectively for as-received and wetted / de-wetted mats. Corresponding inter-fibre spacings, obtained from Eqn.(6), are about 30 nm and 9 nm respectively. The latter figure is broadly consistent with the micrographs shown in Fig.2. In general, the spacings between fibres in the bundles contained in membranes are expected to lie somewhere between these limits. The MIP data in Fig.3, for the homogeneous bundle, also confirm the presence of a narrow range of fine pores (~5-15 nm). This is consistent with the micrograph in Fig.2(b) and it is clear that the simple wetting / dewetting procedure reduces the inter-fibre spacing from ~30 nm to ~10 nm.

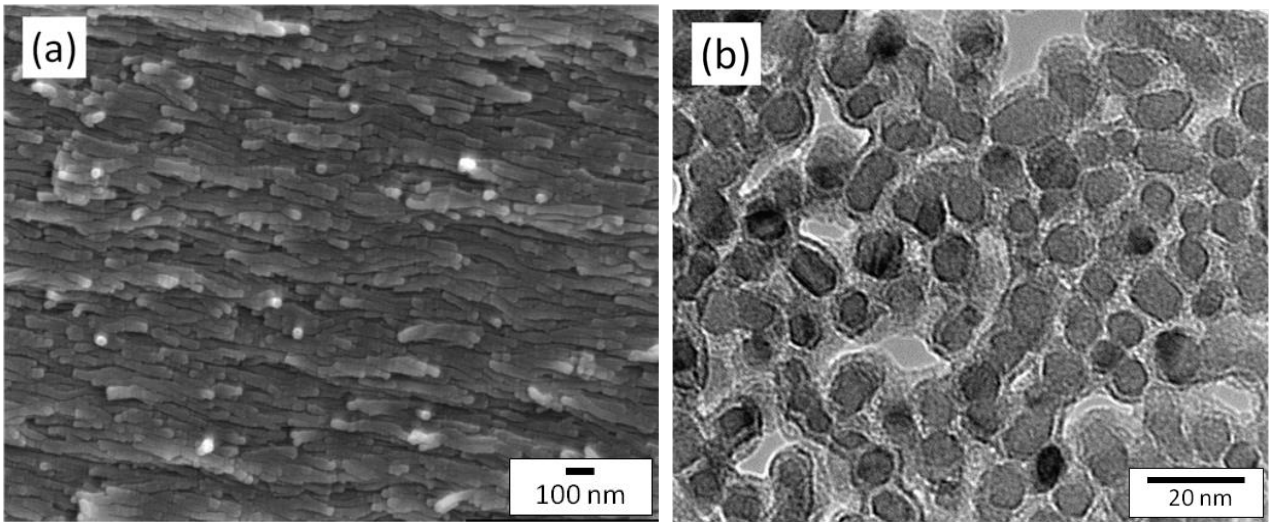

Fig.2 The fibre architecture of a wetted / de-wetted homogeneous fibre bundle, illustrated by (a) an SEM micrograph (plane parallel to the fibre axis) and (b) a TEM micrograph (plane transverse to the fibre axis).

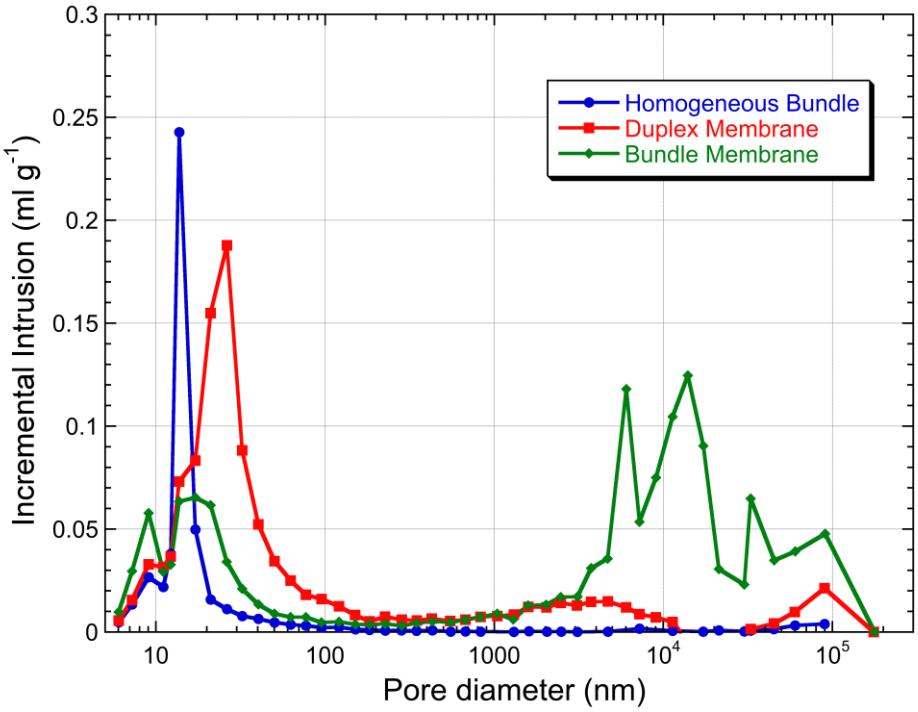

Fig.3 Mercury intrusion porosimetry data for three different fibre architectures.

3.2 Microstructure of Duplex Membranes

The SEM images in Fig.4 illustrate the main features of the membrane structure, produced after extended periods of dispersion in liquid suspension. A two-layer ("duplex") structure was produced, with the lower part comprising well-dispersed fibres and the upper part made up of fibre micro-bundles. Initiation of (vacuum-assisted) drainage induced turbulence in the liquid, with the free (well-dispersed) fibres being pulled towards the support mesh as the liquid flowed downwards, where they formed a smooth, homogeneous layer. The fibre bundles, on the other hand, were unable to move freely through the increasingly fibre-rich liquid and eventually formed the upper layer of the membrane, which has a noticeably rougher appearance.

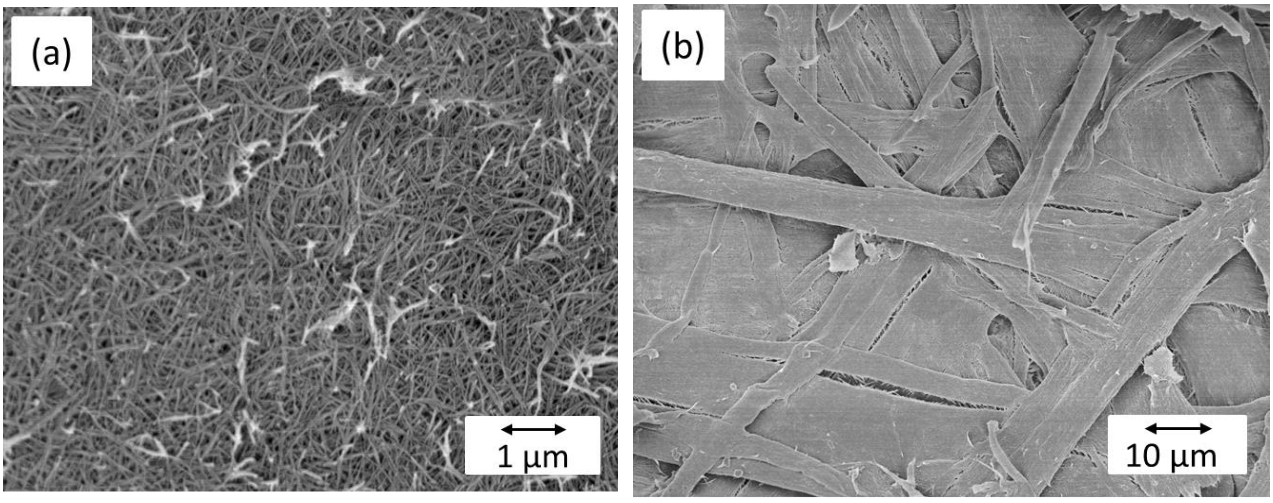

Fig.4 SEM micrographs of the free surfaces of a duplex membrane, showing the appearance of: (a) the homogeneous (lower) layer and (b) the micro-bundle (upper) layer.

Of course, the proportions of the two layers will depend on the degree of dispersion and fragmentation of the fibres during the stirring process. The average fibre length in the micro-bundle layer is considerably higher than that in the homogeneous layer. The MIP data in Fig.3, for the duplex membrane, are consistent with this picture. It can be seen that there are very fine (intra-bundle) pores (in the range 5-20 nm), slightly coarser pores (~20-100 nm) located between fibres in the regions containing dispersed fibres and also some quite coarse pores (~1 – 10 μm) that are presumably the spaces between bundles.

3.3 Microstructure of Bundle Membranes

Membranes made up entirely of micro-bundles (Fig.4(b)) were obtained by using the coarser (100 μm) stainless steel mesh, instead of the 0.2 μm PES mesh. This allowed the dispersed fibres (Fig.4(a)) to pass through, so that there was a substantial (~25%) reduction in fibre retention. SEM examination confirmed that these membranes were comprised solely of micro-bundles. Such micro-bundles have small inter-fibre spacings within them, but coarse porosity between the bundles. This is clear from the MIP plot in Fig.3 for the bundle membrane, which shows coarse pores (in the range 1-100 μm) corresponding to inter-bundle space and fine pores (5-30 nm) corresponding to intra-bundle regions.

3.4 Microstructures of Silica-containing Membranes

SEM images are shown in Fig.5, from duplex and bundle membranes, after silica treatment. It can be seen in Fig.5(a) that the pores between the dispersed fibres (see Fig.4(a)) have been filled (with silica). In Fig.5(b), it is not clear whether the fine intra-bundle spaces have been filled, but it can be seen that the coarse voids between the bundles have mostly remained clear. This is unsurprising, since most of these voids are probably too large to be "bridged" by precipitating silicate.

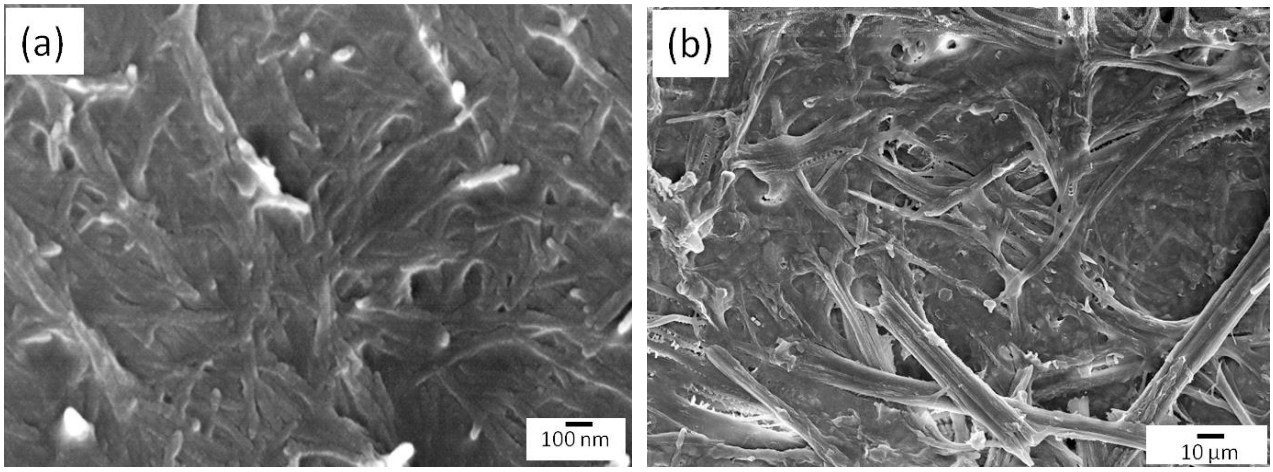

Fig.5 SEM micrographs from free surfaces of: (a) a duplex membrane (underside) and (b) a bundle membrane, after silica incorporation.

Pore size distributions after the addition of silica were analysed using both MIP and gas adsorption, since some of the pores are in this case below the MIP detection limit (~7 nm). The MIP data are shown in Fig.6(a) and the gas adsorption data in Fig.6(b). Since the mathematical models for mercury intrusion and gas adsorption are different, it is not really appropriate to make accurate quantitative comparisons between the two in regions where the pore ranges overlap (7 – 300 nm), although it can be seen that they are qualitatively consistent, as expected [14]. There are clearly two relevant pore size ranges, one corresponding to inter-bundle voids (10 - 100 μm) and the other corresponding to intra-bundle spaces and those between dispersed fibres (2 – 100 nm).

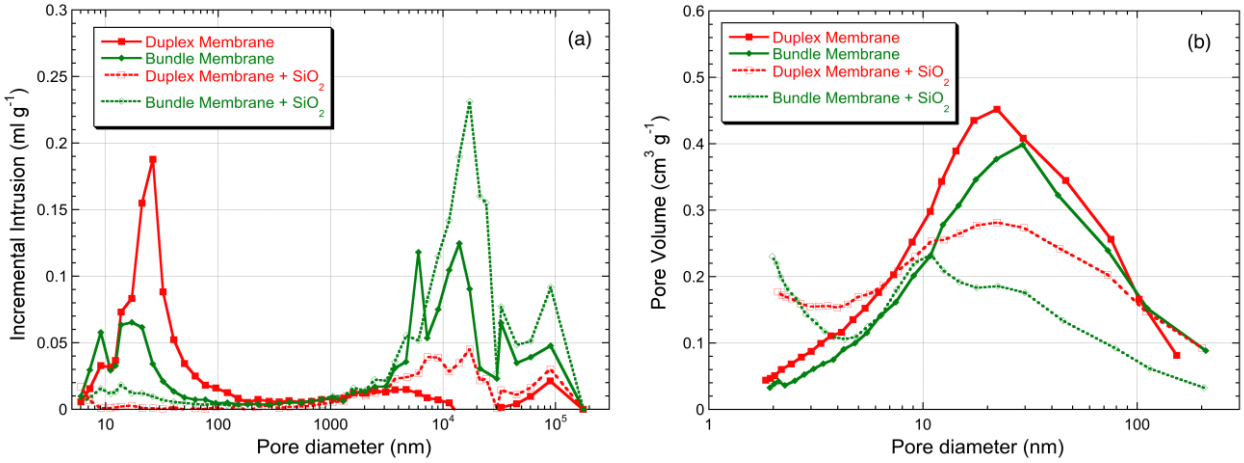

Fig.6 Pore size distributions for duplex and bundle membranes, with and without infiltrated silica, in the form of (a) MIP data (range down to ~7 nm) and (b) gas adsorption data (range ~3-300 nm)

Comparison between solid and dotted lines in Fig.6 reveals the changes in pore size distributions introduced by the presence of the silica. For both types of membrane, the coarse (inter-bundle) void content seemed to have increased, whereas the proportion of finer pores (<50 nm) has decreased. Both of the silica-impregnated membranes were observed to warp slightly after calcination at 500˚C. Although the membranes had previously been sintered at 700˚C, to improve the structural integrity of the fibrous network, the silica treatment appeared to cause some distortion. This is probably responsible for the increase in the coarse voids, although this change was apparently not detrimental to the filtration performance - see §4. It is in any event clear that the silica has formed within the fine inter-fibre interstices, creating in both cases some very fine pores (~3-6 nm). These are probably within the silica, which is expected to have porosity on this scale.

A summary of the surface area and porosity data obtained by gas adsorption is presented in Table I. It can be seen that these data are consistent with the picture that emerges of these pore architectures. Silica addition raised the surface area by 26% for the duplex membranes and by

98% for the bundle membranes. This is indicative of the porous nature of the silica. Introduction of the silica also reduces the average pore diameter for both types of membrane. The pore volume also decreased in both cases. This is again indicative of the formation of silica within the pores in the membrane. It is worth noting at this point that the bundle membranes (containing relatively large inter-bundle voids of ~10 μm, in addition to very fine intra-bundle pores) might be expected to offer attractive combinations of high permeability and fine-scale filtration capability. This concept is illustrated by Fig.7, which shows how fluid flow might be envisaged to take place with such pore architectures.

Fibre network type	Specific surface area (m^2 g^{-1})*	Average pore size (nm)	Specific vol. of pores 1.7-300 nm diameter (cm^3 g^{-1})
Homogeneous Bundles	130	8	0.3
Duplex Membranes	130	13.7	0.5
Silica-infiltrated Duplex Membranes	164	10.8	0.43
Bundle Membranes	109	16	0.44
Silica-infiltrated Bundle Membranes	216	8	0.29

**Calculated specific surface areas for fibres of diameter 8, 9 and 10 nm are respectively 129, 114 and 103* m^2 g^{-1}.

Table I Surface area and porosity data (from gas adsorption measurements) for several types of fibre assembly

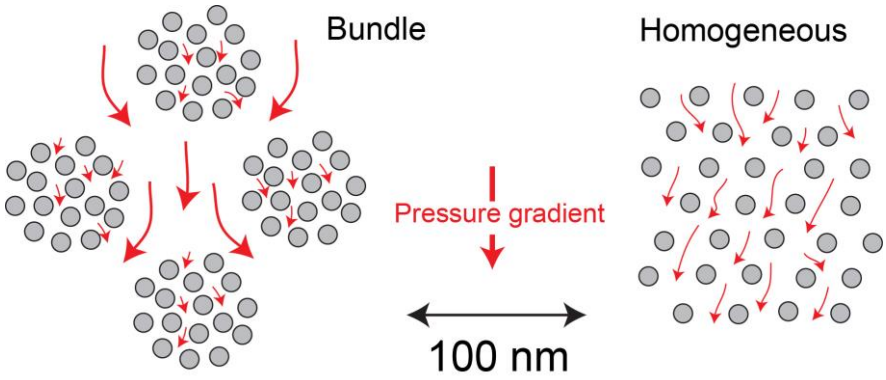

Fig.7 Schematic depiction of how fluid flow is likely to take place within a fibre bundle structure, compared with one that is more homogeneous (and has a similar porosity level and fibre diameter).

From the weight gain after addition of silica to the bundle membrane, the volume fraction of silica was calculated to be ~2.7%. Gas adsorption studies, however, suggested that the volume occupied by the silica was ~4.9% - see the pore volume data in Table I. Given the asymmetric pore size distribution in the membrane scaffold, it can be inferred that there is a higher percentage of silica responsible for pores in the size range concerned (2-300 nm), resulting in a higher estimate using the gas adsorption data. To summarise, about 3 vol% of silica was incorporated

into bundle scaffolds, in which the fibres constituted about 8 vol%. The overall porosity level of the bundle membranes containing silica was thus ~89%.

4 Transport Properties

4.1 Permeability

Experimental data from the permeation studies are summarised in Table II, in which the fibre diameter and volume fraction of each membrane are also presented. Predicted and measured permeability values are shown in Fig.8, in the form of a plot of κ against *f*, with predicted curves shown for fibre diameters of 8 nm and 20 nm. Several points can be noted. Firstly, the experimental permeability values for duplex membranes are more than an order of magnitude lower than the predicted curves. This could be due to special effects associated with such fine pores. Sparreboom et al [17] deduced that, in systems with flow channels smaller than 10 nm, Stokes law [18] may not be applicable and the individual nature of molecules may need to be taken into account. Of course, it should also be appreciated that the Carman-Kozeny equation (Eqn.(5)) only involves the specific surface area (in addition to the porosity level). It thus takes account of the scale of the pores, but not their architecture. For the bundle membranes, on the other hand, the measured permeability is broadly consistent with the predicted curves.

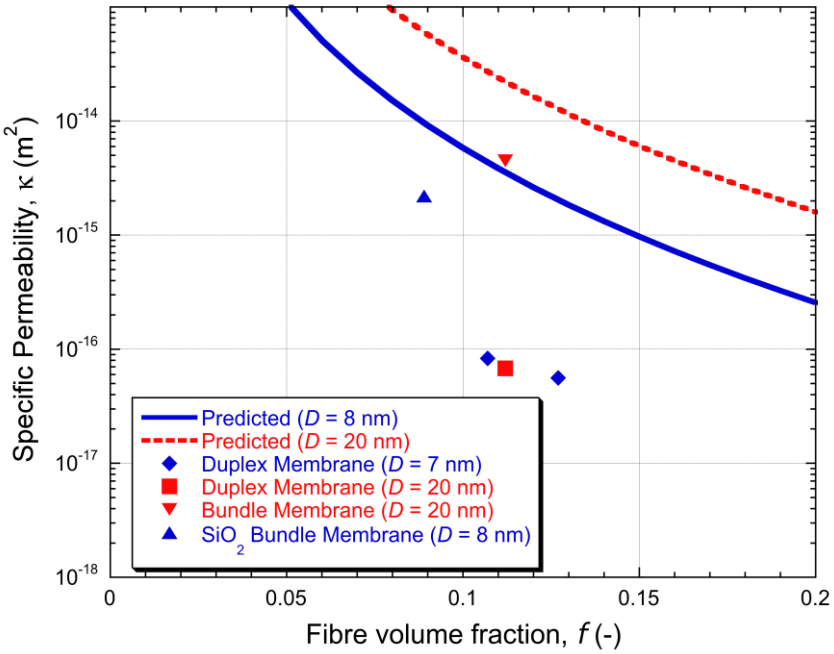

Fig.8 Specific permeability as a function of fibre volume fraction, for several types of membrane, comparing experimental data with predictions obtained using the Carman-Kozeny equation (Eqn.(5)).

Addition of silica (to the bundle membrane) doubled the surface area, as well as reducing the average pore size by half (Table I). However, the permeability is not correspondingly reduced for

this membrane. The inter-bundle voids may largely determine the permeability, with or without infiltration with silica. This concept is illustrated in Fig.7. These larger pores may not necessary compromise filtration efficiency (see below), since there is some flow through the finer pores.

Sample	Fibre diameter D (nm)	Fibre volume fraction f (%)	Specific permeability κ (m^2)
Duplex Membrane (Sample 1)	7	10.7	8.3×10^{-17}
Duplex Membrane (Sample 2)	7	12.7	5.6×10^{-17}
Duplex Membrane (coarse fibre)	20	11.2	6.8×10^{-17}
Bundle Membrane (coarse fibre)	20	11.2	4.5×10^{-15}
Silica-infiltrated Bundle Membrane	8	8.9	2.2×10^{-15}

Table II Measured fibre content and specific permeability values for several types of membrane.

4.2 Filtration Efficiency

A summary of the filtration and separation observations is presented in Table III. After passing solutions of Methylene Blue (a cationic dye, with a molecular diameter of about 2 nm) through both types of membranes, prior to incorporating the silica, the filtrate remained distinctly blue, indicating that they did not remove this dye. This was reported in previous work [8]. However, after incorporation of the silica, both types of membrane did successfully filter out this dye and a visually clear filtrate was collected. This is interesting, particularly for the bundle membrane, since it demonstrates that the inter-bundle voids, while ensuring that the specific permeability was relatively high, did not compromise the filtration efficiency. On the other hand, Trypan Blue (an anionic dye with a larger diameter of ~5 nm), was not filtered by any bundle membranes, including those containing silica. Moreover, Methyl Orange, a small (2 nm) anionic dye, was not filtered by any membrane, duplex or bundle, with or without silica. This suggests that the retention of the Methylene Blue by the silica-containing membranes involves charge-related effects, whereas retention of the Trypan Blue by the duplex membranes is largely mechanical (in the well-dispersed regions).

Membrane Type	Trypan Blue (5 nm, -ive)	Methylene Blue (2 nm, +ive)	Methyl Orange (2 nm, -ive)	MB + MO
Duplex	Yes	No	No	No
Silica-infiltrated Duplex	Yes	Yes	No	Separation
Silica-infiltrated Bundle	No	Yes	No	Separation

Table III Filtration and separation outcomes for three ionic dyes, using three types of membrane. 'No' indicates that the filtrate is of the same colour as the initial dye solution, while 'yes' indicates that the filtrate is clear.

4.3 Separation of Different Dyes in Solution

To check whether these filtration mechanisms operate independently, solutions containing mixtures of cationic and anionic dyes with similar molecular sizes (Methylene Blue and Methyl Orange) were passed through various membranes. This solution was initially green in colour - see Fig.9(c). As illustrated by Fig.9(d), passing it through a silica-containing bundle membrane produced a filtrate that was predominantly orange, showing that, as for the two dyes on their own, the MB was filtered, but the MO was not. This confirms, not only that the mechanism of filtration in this case cannot be purely mechanical, and probably involves electrical charge effects, but also that the filtration processes taking place for the two dyes separately can also operate simultaneously.

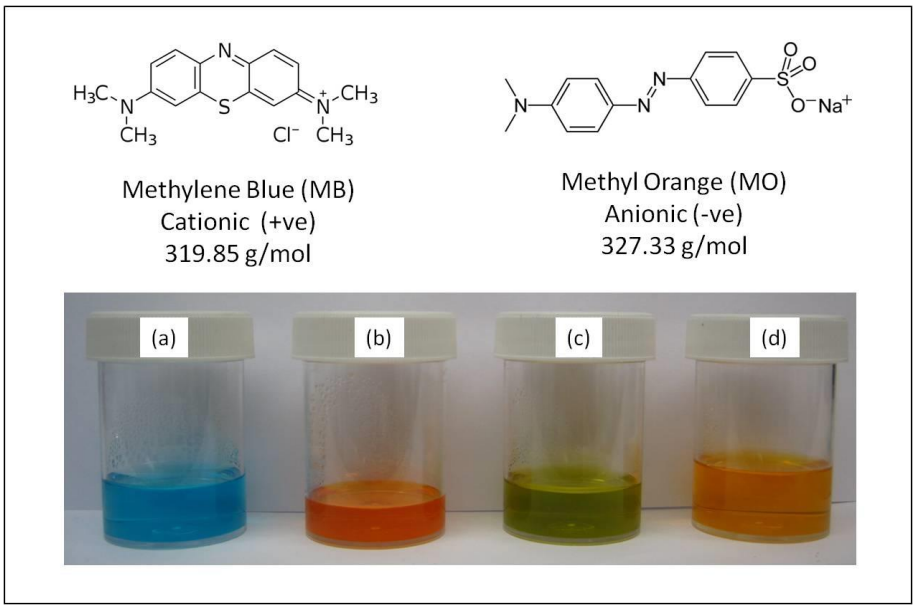

Fig.9 Photos of beakers containing aqueous solutions of: (a) Methylene Blue, (b) Methyl Orange, (c) a mixture of MB and MO and (d) the filtrate produced when such a mixture was passed through a silica-containing bundle membrane.

4.4 Filtration Mechanisms

It seems likely that, at least in some cases, surface electrical effects [19] are playing a significant role effect. Inorganic surfaces tend to become charged and an oppositely-charged region of counter-ions often develops in the liquid [20]. This "screening" region is known as the Electrical Double Layer (EDL), because it consists of two regions of opposite charge, some of which are bound and others mobile [21]. This leads [22] to the 'Exclusion Enrichment Effect' (EEE). The counter-ion that is bound to the surface will exclude counter-ions, but attract co-ions. Thus the centres of pores will tend to become enriched with co-ions. For the system of interest here, the silica is negatively charged and, in an electrolyte, it will attract positively-charged cations to its surface. In a sufficiently narrow channel, this positively-charged inner wall may exclude positive

ions from entering the channel, but allow negatively-charged ions to enter. This effect appears to be responsible for the preferential passage of the negatively charged MO in the experiments described here. From the observed separation of ionic dyes, it can be inferred that the EEE appears to operate effectively for these "hybrid" membranes.

The fact that MB is filtered by silica-containing bundle membranes, while the (larger) TB and (similarly-sized) MO are not, also suggests that cationic dye molecules are preferentially attracted into the (silica-containing) bundles, despite the fact that, overall, these regions will not be charged. Presumably there are mechanisms of the type described above operating at the boundaries between the faster-flowing liquid in the inter-bundle space and that in the pores in the silica within the bundles, whereby entry into these very fine pores is favoured for cationic molecules.

5 Conclusions

The following conclusions can be drawn from this work.

(a) Two types of membrane, termed duplex and bundle, have been produced by sedimentation from aqueous suspension, both based on an ultra-fine alumina fibre. Hybrid membranes were then manufactured by incorporating silica into these two types, using a sol-gel route. A porous silica structure was formed within the (relatively small) spaces within these structures.

(b) A relatively large (anionic) dye, Trypan Blue, is filtered by duplex membranes, which contain a layer in which the fibres are well-dispersed and have uniformly fine pores (of similar size to the molecular diameter) between them. This happens with or without the presence of the silica. It seems likely that removal of this dye occurs predominantly by mechanical entrapment in the uniform layer. On the other hand, bundle membranes, which are composed of fibre bundles separated by relatively large pores, do not filter this dye, with or without silica present.

(c) Both types of hybrid membrane effectively filter Methylene Blue (cationic) dye from aqueous solution. They were also effective in separating it from an anionic dye, Methyl Orange. Since these dyes have similar molecular sizes (~2 nm diameter), mechanical entrapment alone cannot account for this differential filtration effect. It is concluded that this separation of dyes is primarily due to an Exclusion-Enrichment Effect (EEE), as a result of the electrical double layer (EDL) formed on the interface between the silica and the liquid.

(d) Measured specific permeabilities were ~10^{-17} m^2 for silica-containing duplex membranes, and ~10^{-15} m^2 for silica-containing bundle membranes. The latter thus allow higher flow rates during filtration, giving, for example, a flux of about 210 litres m^{-2} h^{-1} for a pressure drop of 0.1 bar across a membrane of thickness 300 μm. This combination of high permeability and good filtration efficiency is thought to arise from the multi-scale architecture of such bundle membranes, with flow predominantly through coarse inter-bundle pores, but with sufficient flow through fine intra-bundle pores to ensure good filtration.

Acknowledgements

Financial support for this work has been provided by Trinity Hall College, Cambridge and the Cambridge Commonwealth Trust. The authors would also like to acknowledge the assistance of Metallurg Engineering Ltd, particularly Dr. Michael Terehov, in supplying fibres and providing technical information. The authors are also grateful to Dr. Natalia Tabachkova, from the National University of Science and Technology in Moscow (MISIS), for kindly supplying the TEM image shown in Fig.2(b).

References

[1] Lin, YS, *Microporous and Dense Inorganic Membranes: Current Status and Prospective.* Separation and Purification Technology, 2001. **25**: p.39.

[2] Ockwig, NW and TM Nenoff, *Membranes for Hydrogen Separation.* Chemical Reviews, 2007. **107**: p.4078.

[3] Nair, BN, *Sol-Gel Synthesis of Molecular Sieving Silica Membranes.* Journal of Membrane Science, 1997. **135**: p.237.

[4] Benito, JM, A Conesa, and MA Rodriguez, *Preparation of Multilayer Ceramic Systems for Deposition of Mesoporous Membranes.* Journal of Materials Science, 2005. **40**: p.6105.

[5] Yoshino, Y, *Development of Tubular Substrates, Silica-based Membranes and Membrane Modules for Hydrogen Separation at High Temperature.* Journal of Membrane Science, 2005. **267**: p.8.

[6] Clyne, TW, AE Markaki, and JC Tan, *Mechanical and Magnetic Properties of Metal Fibre Networks, with and without a Polymeric Matrix.* Composites Science and Technology, 2005. **65**(15-16): p.2492-2499.

[7] Ke, X, Z Zheng, H Zhu, L Zhang, and X Gao, *Metal Oxide Nanofibres Membranes Assembled by Spin-coating Method.* Desalination, 2009. **236**: p.1-7.

[8] Su, VMT, M Terehov, and TW Clyne, *Filtration Performance of Membranes Produced Using Nanoscale Alumina Fibres (NAF).* Advanced Engineering Materials, 2012. **14**(12): p.1088-1096.

[9] Zhao, D, P Yang, N Melosh, J Feng, BF Chmelka, and GD Stucky, *Continuous Mesoporous Silica Films with Highly Ordered Large Pore Structures.* Advanced Materials, 1998. **10**(16): p.1380-1385.

[10] Wu, YY, *Composite Mesostructures by Nano-confinement.* Nature Materials, 2004. **3**: p.816.

[11] Brinker, CJ, *Evaporation-Induced Self-Assembly: Nanostructures Made Easy.* Advance Materials, 1999. **11**(7): p.579.

[12] Brunauer, S, PH Emmett, and E Teller, *Adsorption of Gases in Multimolecular Layers.* Journal of the American Chemical Society, 1938. **60**: p.309-319.

[13] Barrett, EP, LG Joyner, and PP Halenda, *The Determination of Pore Volume and Area Distributions in Porous Substances. 1. Computations from Nitrogen Isotherms.* Journal of the American Chemical Society, 1951. **73**: p.373.

[14] Webb, PA and C Orr, *Analytical Methods in Fine Particle Technology,* 1997: Micromeritics Instrument Corporation.

[15] Carman, P, *Flow of Gases Through Porous Media,* 1956, London: Butterworths Scientific Publications. 182.

[16] Valdes-Parada, FJ, JA Ochoa-Tapia, and J Alvarez-Ramirez, *Validity of the permeability Carman□Kozeny equation: A volume averaging approach.* Physica A: Statistical Mechanics and its Applications, 2009. **388**: p.789□798.

[17] Sparreboom, W, A van den Berg, and JCT Eijkel, *Transport in Nanofluidic Systems: A Review of Theory and Applications.* New Journal of Physics, 2010. **12**: p.015004.

[18] Fox, RW and AT McDonald, *Introduction to Fluid Mechanics*. 3rd ed1985, New York: Wiley.

[19] Eijkel, JCT, *Scaling Revisited.* Lap on a Chip, 2007. **7**: p.1630.

[20] Schoch, RB, JY Han, and P Renaud, *Transport Phenomena in Nanofluidics* Reviews of Modern Physics, 2008. **80**(3): p.839.

[21] Israelachvili, J, *Intermolecular and Surface Forces*. 2nd ed., 2005, London, UK: Elsevier Academic Press.

[22] Plecis, A, RB Schoch, and P Renaud, *Ionic Transport Phenomena in Nanofluidics: Experimental and Theoretical Study of the Exclusion-Enrichment Effect on a Chip.* Nanoletters, 2005. **5**(6): p.1147-1155.

Fig.1
Click here to download Production Data: fig_1_schem_perm_meas.jpg

Fig.2a

Click here to download Production Data: fig_2a_SEM NAF Bundle.jpg

Fig.2b

Click here to download Production Data: fig_2b_TEM NAF Bundle.jpg

Fig.3
Click here to download Production Data: fig_3_MIP.tif

Fig.4a

Click here to download Production Data: fig_4a_SEM fine fibre dispersion.jpg

Fig.4b

Click here to download Production Data: fig_4b_Micro bundled dispersion.jpg

Fig.5a
Click here to download Production Data: fig_5a_NAFM-Si.jpg

Fig.5b
Click here to download Production Data: fig_5b-BM-Si.jpg

Fig.6a

Click here to download Production Data: fig_6a_MIP with silica.tif

Fig.6b
Click here to download Production Data: fig_6b_gas+silica.tif

Fig.7
Click here to download Production Data: fig_7_fluid flow schem.jpg

Fig.8

Click here to download Production Data: fig_8_kappa(f) membranes.tif

Fig.9
Click here to download Production Data: fig_9_Separation_MB_MO.jpg